ORCA – Online Research @ Cardiff

Accepted Manuscript

In situ assessment of the fabric and energy performance of five conventional and non-conventional wall systems using comparative coheating tests

Eshrar Latif, Mike Lawrence, Andy Shea, Pete Walker
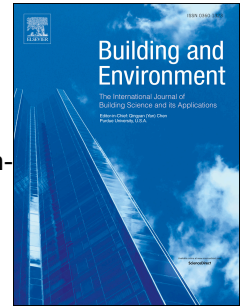
Please cite this article as: Latif E, Lawrence M, Shea A, Walker P, In situ assessment of the fabric and energy performance of five conventional and non-conventional wall systems using comparative coheating tests, *Building and Environment* (2016), doi: 10.1016/j.buildenv.2016.09.017.

This is a PDF file of an unedited manuscript that has been accepted for publication. As a service to our customers we are providing this early version of the manuscript. The manuscript will undergo copyediting, typesetting, and review of the resulting proof before it is published in its final form. Please note that during the production process errors may be discovered which could affect the content, and all legal disclaimers that apply to the journal pertain.

In situ assessment of the fabric and energy performance of five conventional and non-conventional wall systems using comparative coheating tests

Eshrar Latif[1], Mike Lawrence, Andy Shea, Pete Walker

BRE Centre for Innovative Construction Materials, Department of Architecture and Civil Engineering, University of Bath, BA2 7AY, UK

Abstract

Comparative coheating tests have been carried out in five test buildings with walls constructed of Concrete Block Masonry and timber framed Hemp-lime composite, Polyisocyanurate (PIR), Wood Fibre and Mineral Wool. Five different methods of determining heat loss coefficient (HLC) were applied during the data analysis. While some variability in HLC values was observed between the different forms of construction, the hierarchy of HLC values among the test buildings were consistent, with the Concrete Block Masonry exhibiting the highest and Wood Fibre test building exhibiting the lowest HLC values. Except for the Concrete Block Masonry, there was good agreement between the calculated HLC values and those derived by applying the method 5 where the analysis incorporated both the effects of solar radiation and thermal mass. The in-situ U-value for the Concrete Block wall, determined by the average method, was 32.8% higher than its design value, whilst the other wall systems showed marginally lower U-values than their corresponding design U-values.

Key words: Coheating test, U-value, in-situ test, bio-based insulation materials, hemp-lime, wood fibre insulation, thermal conductivity.

1. Introduction

The building sector contributes to approximately 30% of global total energy consumption, of which nearly two-thirds can be attributed to the combined energy use of space heating, space cooling and water heating [1]. In response to this, a number of regulations have been introduced worldwide with the aim of reducing energy use in domestic and non-domestic buildings; these regulations include the Energy Performance Building Directive [2], the Energy Efficiency Directive [3] in the European Union, and Part L of the Building Regulations [4] in the UK.

---

[1] Corresponding author. E-mail address: latife@cardiff.ac.uk (E. Latif).

The aforementioned regulations use certain prediction methods to assess the building energy use during the design stage. Evidences suggest that there is a discrepancy between the predicted and actual energy use in the buildings [5] , the mismatch is broadly referred to as the 'energy performance gap' [6]. The 'energy performance gap' between the actual energy use and the calculated energy use of buildings is subject to scores of academic discussions [5-13]. Sometimes the amount of discrepancy is reported as 100% or more   [5], e.g., Erhorn [12] reported a performance gap of 300%. The reasons for this 'energy performance gap' is widely attributed to poor prediction of actual energy use (design stage), poor quality of construction, poor service design, discrepancy between design specification and the specification of the construction as-built (construction stage) and user behaviour and 'Rebound Effect' (operational stage) [8, 9]. While, user behaviour remains the most reported key reason for energy performance gap [14-16] , Gorse et al. [13] observed that poor thermal performance of building fabric could also be an important contributor to unpredicted energy use.

In addition to operational energy, embodied energy of buildings also contributes to their total lifetime carbon emissions. About 6-20% energy use of a conventional building and about 74-100% of that of a nearly zero energy building is attributed to embodied energy [17]. By 2020 all new buildings in the EU countries are required to be nearly zero-energy buildings [2]. It implies that, by 2020, the role of embodied energy will be significant in terms of a building's total energy use. The embodied energy in a building can be reduced by using materials derived from renewable sources as they generally require less 'extraction', processing and transportation energy [18]. In general, locally produced bio-based building materials carry less embodied energy than the fossil fuel and mineral based building materials [19].

Bio-based building materials, especially insulations and envelope-integrated insulation materials, are produced from renewable sourced and show excellent hygric and good to moderate thermal performance [20-22]. Takano et al. [23], in their study on the energy performance of a hypothetical building model in Finland, observed that the life cycle energy balance of the cellulose fibre insulation was the lowest among all building materials including EPS (expanded polystyrene) and glass wool insulations. Latif et al. [20] studied hygrothermal properties of composite fibrous insulations based on hemp and wood-hemp insulation which are highly sustainable [24] and carbo-negative materials. The insulations demonstrated excellent moisture management capacity and similar thermal conductivity to that of mineral wool insulation. Another important bio-based composite material is hemp-lime which is comprised of hemp shiv, the woody core of hemp plant, and a lime based binder [25]. Hemp-lime can be used in walls, floors and roofs. It has 'Excellent' moisture buffer capacity [21] and moderate thermal properties [26]. Apart from plant sources, bio-based materials are also derived from animal sources. Sheep wool insulation is an animal-based renewable bio-insulation with self-extinguishing capacity [27]. Sheep wool insulation demonstrates high moisture buffering capacity and low thermal conductivity [27]. The following bio-based insulation materials also possess broadly similar hygrothermal characteristics as discussed above: straw, flax, wood fibre.

Recently, as part of the Hempsec Project [28], a new wall system is developed to address the concern with both operational and embodied energy use [29]. The panel is called 'HempCell' and the core materials of the panel are hemp-lime and natural fibre such as wood fibre or hemp fibre. While hemp-lime exhibits excellent hygric and moderate thermal resistance properties [21], both hemp and wood fibre exhibit

excellent hygric capacity and good thermal resistance property [20, 30]. As a prefabricated and pre-dried system, HempCell is expected to exhibit optimal thermal performance from the very day of its installation as opposed to the unpredictable and poorer initial thermal performance associated with the in situ cast hemp-lime system.

To compare the thermal performance of the 'HempCell' wall system with the other conventional and emerging wall systems, comparative coheating tests were carried out among five test buildings built with the following walls systems: Concrete Block Masonry, HempCell, Polyisocyanurate (PIR), Wood Fibre and Mineral Wool. A coheating test applies a quasi-steady state method for determining the whole building energy performance [31]. It is typically carried out by elevating the internal temperature to 25°C for a period of 1-3 weeks [32]. The performance is measured in terms of energy use for unit temperature difference between the inside and outside of the building and referred to as heat loss coefficient (HLC). The method for conducting a coheating test is briefly discussed in section 3. In addition to the coheating tests, the wall systems were also compared in terms of the deviation of their in-situ U-value from the corresponding calculated U-values. Assessing the thermal performance of the envelope of an existing building by determining its in situ U-value is a well-established non-destructive method. Desogus et al. [33] compared the results of R value of a wall determined by in situ measurement method and by numerical method. The numerical method used known thermal conductivity of the component materials of the wall as the basis of calculation. They concluded that there was no significant difference between the results obtained as long as the internal and external temperature difference was more than 10K during the in situ test. In a similar line of study, Evangelisti et al. [34] observed that the calculated U-

value of a wall could, however, vary from the in situ U-value of an envelope if the assumption of thermal conductivity of the component materials were inaccurate.

2. Test buildings, wall systems and instrumentation

2.1. The test buildings and instrumentation

Five test buildings, with five different wall systems, were constructed at the Building Research Park, Wroughton, UK, which hosts the HIVE experimental building facility [35] (Fig. 1). The five wall systems are: Concrete Block Masonry; timber framed wall panels containing HempCell; PIR (polyisocyanurate); Wood Fibre; and Mineral Wool insulations. Typical plans and sections of the five test buildings are shown in Fig. 2 with the corresponding dimensions being presented in Table 1. All the timber frame wall systems were designed to achieve the identical U-value of 0.15 W/m^{2}K using BS EN ISO 6946:2007 [36]. The Concrete Block Masonry was also designed to achieve an U-value of 0.15 W/m^{2}K but a detailed calculation by the authors using BS EN ISO 6946:2007 [36] and including the effect of thermal bridges through mortar joints and metal ties showed that the design U-value was 0.19 W/m^{2}K. Floors and ceilings of the test buildings were of identical construction with a design U-value of 0.10 (W/m^{2}K).

Fig. 1. The five test buildings at wroughton, from left to right: HempCell, Mineral Wool, PIR, Wood Fibre, Concrete Block Masonry.
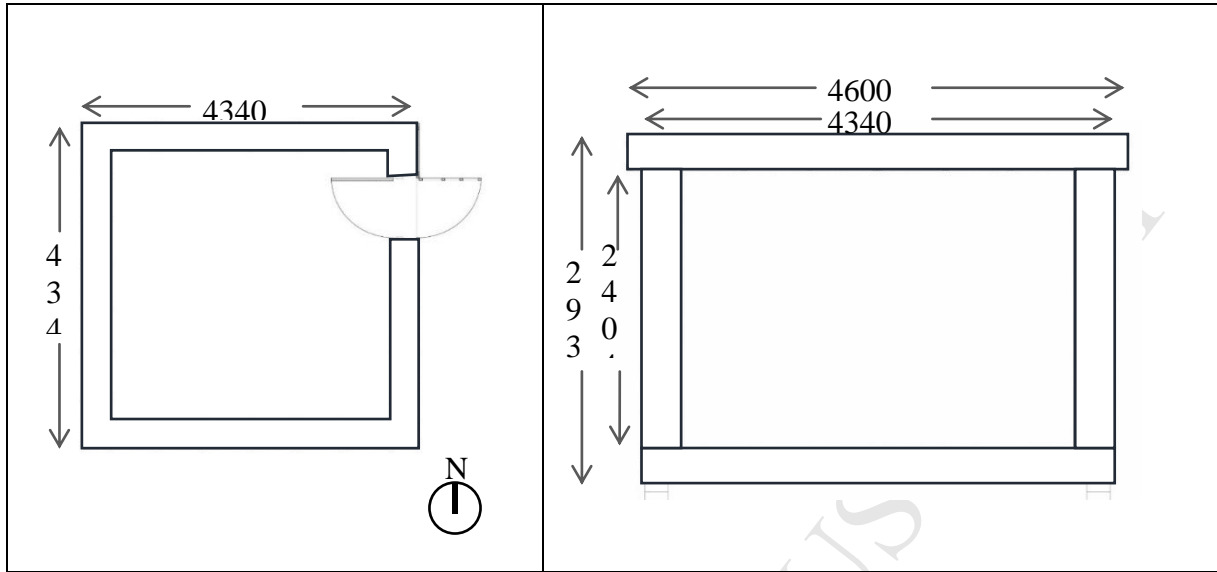

Fig. 2. External dimension of a typical test buildings, left: plan, right: section.

Table 1. Internal and external dimensions of the test buildings.

Test buildings	External Length/ Width (m)	External Area (m²)	External Height floor to roof) (m)	Internal Length/ Width (m)	Internal Area (m²)	Internal Height (m)	Internal volume
Concrete Block Masonry	4.34	18.84	2.94	3.54	12.53	2.4	30.08
HempCell	4.34	18.84	2.94	3.6	12.96	2.4	31.10
PIR	4.34	18.84	2.94	3.82	14.59	2.4	35.02
Wood Fibre	4.34	18.84	2.94	3.63	13.16	2.4	31.60
Mineral Wool	4.34	18.84	2.94	3.73	13.91	2.4	33.38

2.2. The wall systems and instrumentation

Some key details of the structure of the wall systems are provided in Table 2.

Table 2. Details of the structural systems

Test Buildings	Structural System	Stud Size (mm X mm)	Stud Spacing centre to centre (mm)	Wall Thickness (mm)
Concrete Block Masonry	Lightweight cavity wall	N/A	N/A	400

HempCell	Timber frame	Outer flange 46X46, Inner flange 46X120, 300 x 9 OSB gussets placed at 1/3 and 2/3 stud height	600	371.5
PIR	Timber frame	Outer flange N/A Inner flange 38X140	600	265
Wood Fibre	Timber frame	219 X 50	600	360
Mineral Wool	Timber frame	Outer flange N/A Inner flange 45X120	600	317.5

One of the key objectives of the coheating experiment was to compare the HempCell (Fig. 3) panel with other conventional and emerging wall systems in terms of energy use and thermal performance. As such, a number of test panels of each test building were instrumented with temperature and relative humidity (RHT) sensors (Figs. 4-8). For temperature sensing, Betatherm thermistor [37] sensors with an accuracy of ± 0.2% were used. For relative humidity sensing, HIH400 sensors [38] with an accuracy of ± 3.5% were used. In the HempCell test building, one panel in each orientation was instrumented. For other test buildings, only wall panels facing North and South were instrumented with RHT sensors. In addition to these, two Hukseflux heat flux sensors [39], with an accuracy of ± 5%, were installed on the inner surface of the North wall of each test building.
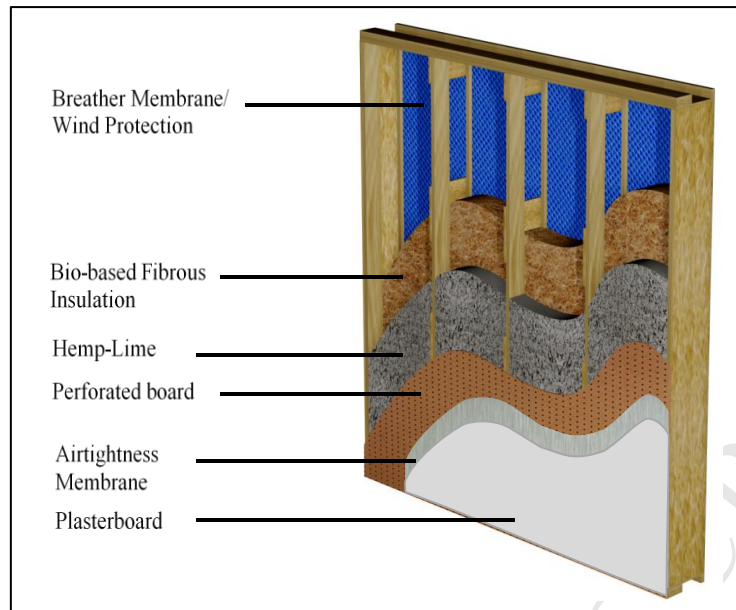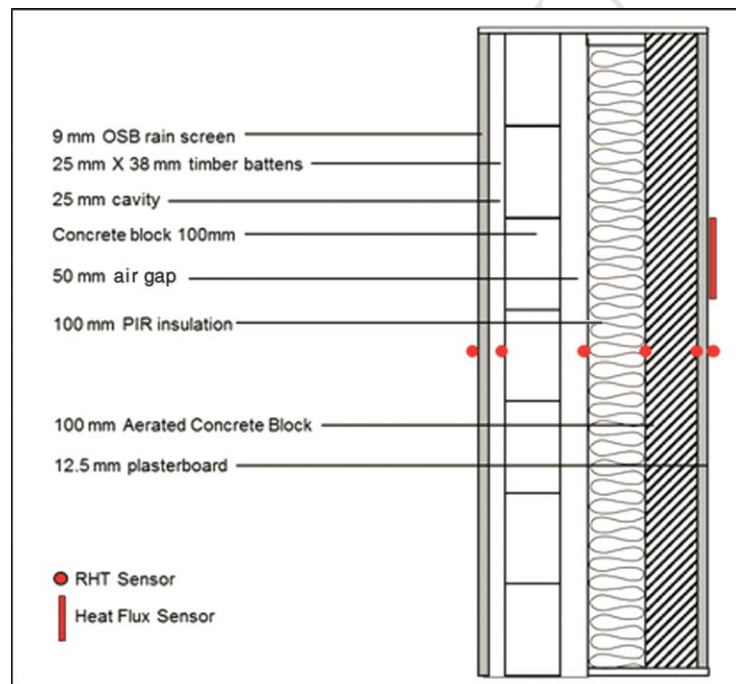
Breather Membrane/
Wind Protection

Bio-based Fibrous
Insulation

Hemp-Lime

Perforated board

Airtightness
Membrane

Plasterboard

Fig. 3. The hempCell panel.

9 mm OSB rain screen

25 mm X 38 mm timber battens

25 mm cavity

Concrete block 100mm

50 mm air gap

100 mm PIR insulation

100 mm Aerated Concrete Block

12.5 mm plasterboard

● RHT Sensor

▮ Heat Flux Sensor

Fig. 4. Vertical section of the Concrete Block Masonry wall.

9 mm OSB outer frame
9 mm OSB rainscreen
25 mm X 38 mm timber battens
25 mm cavity

180 mm wood fibre
220 mm X 50 mm timber batten
120 mm Hemp-lime

25 mm cavity
25 mm X 38 mm timber batten
12.5 mm plasterboard

● RHT Sensor

▌ Heat Flux Sensor
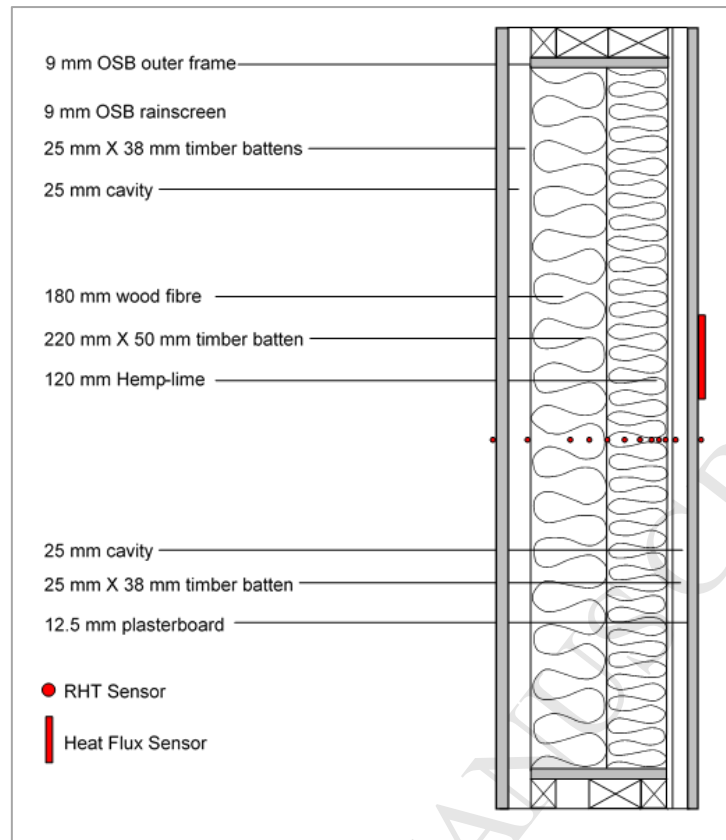
Fig. 5. Vertical section of the HempCell wall.

9 mm OSB outer frame
140 mm 38 mm timber frame
for 140 mm X38 mm timber stud
9 mm OSB rain screen
25 mm X 38 mm timber battens
25 mm cavity
70 mm PIR Insulation
Breather membrane
9 mm OSB racking board
70 mm PIR insulation
25 mm X 38 mm timber batten
Vapour control membrane
45 mm cavity
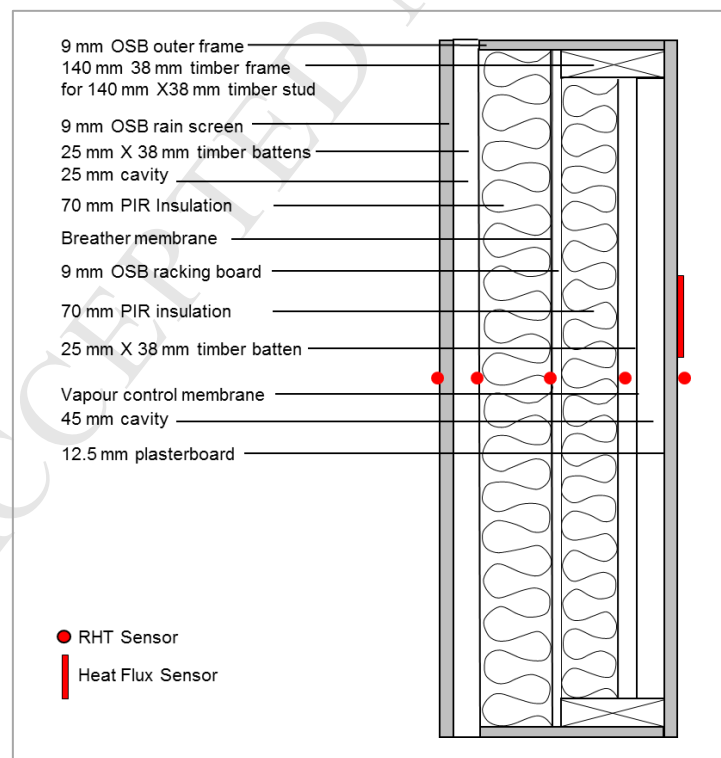12.5 mm plasterboard

● RHT Sensor

▌ Heat Flux Sensor

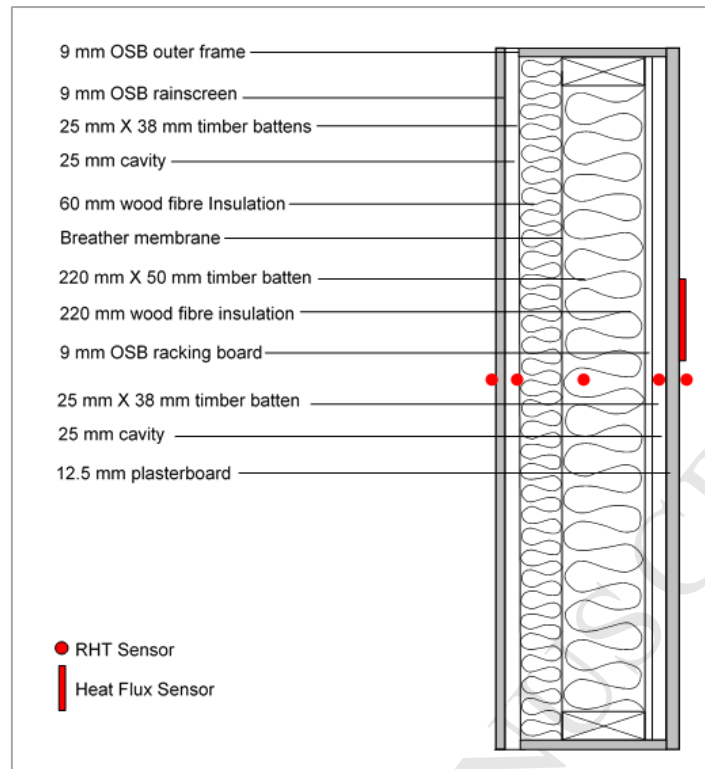**Fig. 6.** Vertical section of the PIR wall.

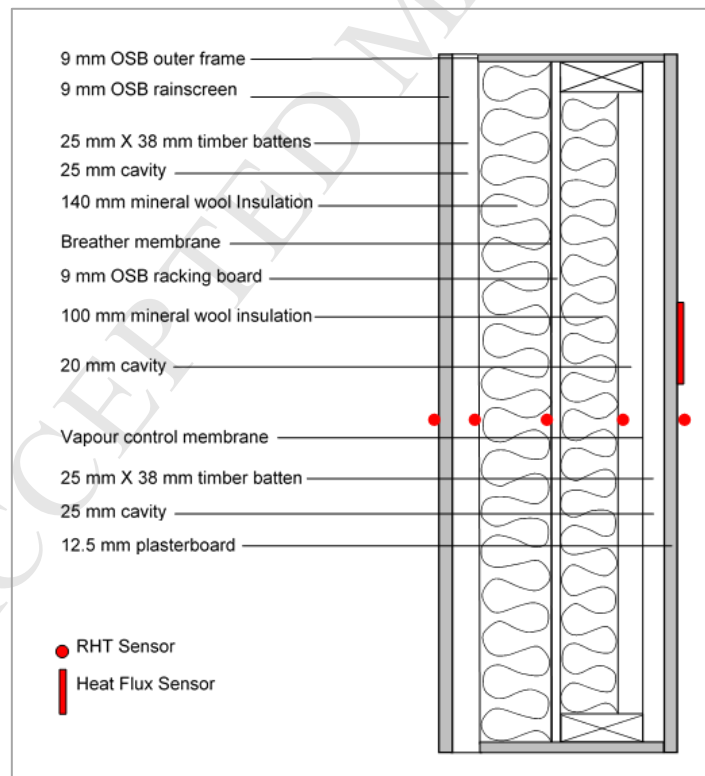**Fig. 7.** Vertical section of the Wood Fibre wall.

Fig. 8. Vertical section of the Mineral Wool wall.

3. Method

3.1. Coheating test method

To determine the HLC values, the unoccupied test buildings were heated to an elevated mean internal temperature of 25°C± 0.5°C, each building employing an electric resistance heating system rated at 0.7 kW for space heating and energy use was monitored using an energy meter with a pulse output of 2000 impulse per kilowatt-hour (2000 imp/kWh). The interiors of the test buildings were maintained at the aforementioned steady temperature for a period of 18 days during the winter month of February 2016. The key external boundary conditions during the test period are presented in Fig. 9.
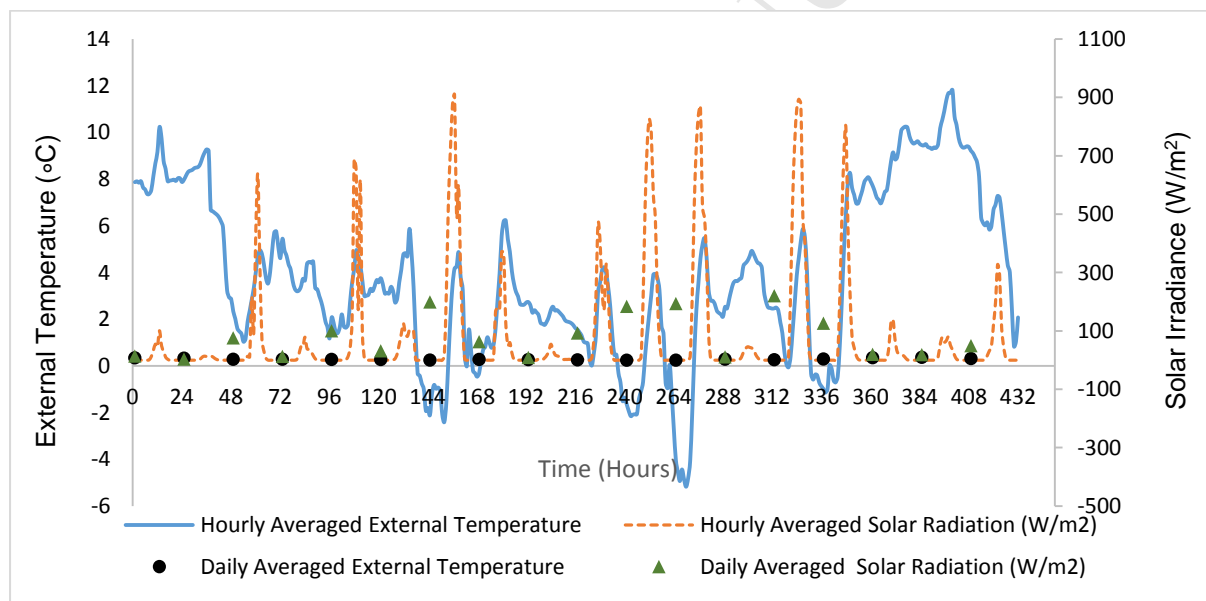

Fig. 9.External temperature and solar radiation during the test.

By measuring the amount of electrical energy required to maintain the elevated mean internal temperature over the test period, the daily heat input (in Watts) to the dwelling was determined [32]. At its simplest form, the heat loss coefficient (W/K) for the test building was calculated by plotting the heat input against the difference in temperature between the interior and exterior of the dwelling (ΔT), given that ΔT is 10K or more. For a better estimation of the HLC, different methods of data analysis

are suggested by a number of researchers [7, 40]. The key methods employed in the present research are described in subsection 3.2.

Heat loss from infiltration was also determined and subtracted from the total heat loss calculation. This was necessary to compare the fabric-only heat loss performance of the five separate test buildings that exhibited varying degree of infiltration rates. The infiltration rates were determined by conducting blower door tests at 50 Pascal pressure difference; a detailed method of the test can be found in the users' manual of 'The Energy Conservatory' [41]. The infiltration rates of the test buildings in air change per hour (ACH) are shown in Table 3.

Table 3. Infiltration rates of the test buildings.

	Concrete Block Masonry	HempCell	PIR	Wood Fibre	Mineral Wool
Infiltration rate (ACH)	0.86	0.59	1.01	0.95	0.95

3.2. Analysis of the coheating data

3.2.1. Method 1

Method 1 is based on the following equation:

$$E = HLC.\Delta T \qquad [1]$$

Where:

E is the daily average heat Input (W),

HLC is the envelope heat loss coefficient (W/K),

ΔT is the daily average temperature difference (K) between the interior and exterior.

In general, researchers [7, 32, 40, 42] incorporate infiltration heat loss into the daily average heat input as a necessary part of the HLC determination. On the contrary, there are also example of decoupling infiltration heat loss from fabric heat loss in the coheating tests [40, 43]. For the purposes of the fabric performance evaluation and comparison, including infiltration heat loss in the HLC is problematic as it will misrepresent the values of envelope heat loss coefficient. This is because different test buildings exhibited significantly varying degree of infiltration rates despite the target infiltration rate being 0.6 air change per hour (ACH) or less. Therefore, in the present paper, E is the infiltration corrected heat input. The equation for infiltration corrected heat input is:

$$E = E_{Total} - E_v \qquad [2]$$

Where:

E_{Total} is the total heating input of the heating equipment

E_v is infiltration heat loss

The infiltration heat loss was calculated using the following equation and factors as presented in the Passivhaus methodology [44]:

$$\text{Infiltration Heat Loss } E_v = V_v . n_{vres} . c . \Delta T \qquad [3]$$

Where:

V_v = Ventilation volume of air (m^3) based on TFA (treatable floor area),

n_{vres} = infiltration (1/h) adjusted to ventilation volume,

$n_{vres} = e.n_{50}.(V_{n50}/V_v)$,

e = shelter factor (typically 0.07), to convert test pressure difference (50 Pa) to typical pressure difference (between 3 to 5 Pa),

c= heat capacity of air, 0.33 Wh/m^{3}K,

ΔT= Air to air temperature difference between indoor and outdoor,

In Method 1, both day and night time data are considered in the analysis and calculation.

3.2.2. Method 2

Method 2 is similar to Method 1 except that only night-time data are used for the HLC analysis to eliminate the effect of solar gain. However, for buildings with high thermal mass, it may be difficult to completely remove the effect of solar gain due to thermal lag.

3.2.3. Method 3

Method 3, also known as the Siviour Method [43], is derived from the following equation:

$$E=HLC.ΔT-A.S \qquad\qquad [4]$$

Where:

E, HLC and ΔT are as defined earlier,

S is the daily average solar irradiance on a south facing vertical plane (W/m^2),

A is the effective solar aperture of the envelope in that plane (m^2).

By dividing both sides of Equation 4 by ΔT, the following equation is derived:

$$E/ ΔT = HLC -A*S/ ΔT \qquad\qquad [5]$$

S/ ΔT is an independent variable and E/ ΔT is a dependent variable. Plotting E/ ΔT against S/ ΔT will provide the value for HLC as a constant and A as the slope.

3.2.4. Method 4

Multiple linear regression based on equation 4, by considering E as a dependent variable and both ΔT and S as independent variable provides value for HLC and A as coefficients of ΔT and S, respectively. Multiple regression analysis was done on the average daily data of ΔT, S and E.

3.2.5. Method 5

Method 5 is based on the following modification of Equation 1:

$$E = HLC.\Delta T_{a.Effective} \qquad [6]$$

Where:

$\Delta T_{a.Effective}$ attempts to incorporate both the effects of solar radiation and thermal mass in ΔT.

$\Delta T_{a.Effective}$ was constructed in two stages. Firstly, the effective external temperature was determined by taking into account the effect of solar radiation gain and long wave radiation exchange. The following equation was used:

$$T_{a.Effective} = T_a + (A*S/(h_{ce}+h_{re})) - ((e_s.C_b.F_{sky}.F_{T.sky}(T_a-T_{sky})(1-c))/(h_{ce}+h_{re})) \qquad [7]$$

Where:

T_a is measured external air temperature (°C),

h_{ce} is external convective surface heat transfer coefficient,

h_{re} is radiative surface heat transfer coefficient,

e_s is emissivity of the external wall surface,

C_b is the black body constant, 5.67 W/m^{2}K^4,

.F_{sky} is angle radiation factor between the surface and the sky,

$F_{T.sky}$ is temperature radiation factor,

T_{sky} is Sky temperature (K),

c is cloud factor, 0 for a clear sky and 1 for a completely overcast sky.

Secondly, the effect of thermal mass is addressed by considering that $\Delta T_{a.Effective}$ is dependent not only on $T_{a.Effective}$ of current time step t, but also on that of the previous time step t-1. As such an average of $T_{a.Effective}$ of time step t and t-1 is used in resolving $\Delta T_{a.Effective}$. The linear regression was conducted on the processed data with a one-hour time step.

3.3. Heat flux data analysis for determining in situ U-value

3.3.1. Numerical calculation

The calculations of the U-value (thermal transmittance) of wall panels are based on BS EN ISO 6946:2007 [36] . The methods are detailed below:

a) Calculation of the U-value of wall panels consisting of homogeneous layers:

The total thermal resistance, R_T, of a plane building component consisting of thermally homogeneous layers perpendicular to the heat flow is calculated by the following equation:

$$R_T = R_{si} + R_1 + R_2 + \ldots + R_n + R_{se} \qquad\qquad [8]$$

where:

R_{si} is the internal surface thermal resistance

$R_1, R_2...R_n$ are the design thermal resistance of each layer

R_{se} is the external surface thermal resistance

(b) Calculation of the U-value of wall panels consisting of homogeneous and inhomogeneous layers

The total thermal resistance, R_T, of a building component consisting of homogeneous and inhomogeneous layers parallel to the surface is expressed as the mean of the upper and lower limits of the resistance:

$$R_T = (R'_T + R''_T)/2 \qquad\qquad [9]$$

Where:

R'_T is the upper limit of total thermal resistance

R''_T is the lower limit of total thermal resistance.

R'_T, is determined by the following equation:

$$1/ R'_T = f_a/ R_{Ta} + f_b/ R_{Tb} +\ldots+ f_q/ R_{Tq} \qquad\qquad [10]$$

Where:

$R_{Ta}, R_{Tb}\ldots R_{Tq}$ are the thermal resistances of each section,

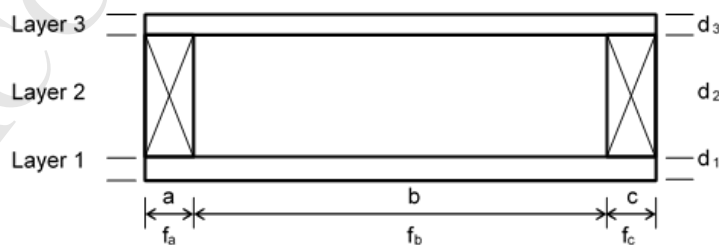$f_a, f_b\ldots f_q$ are the fractional areas of each section (Fig.10).

Fig. 10. Horizontal cross-section of a notional wall panel [45].

The equivalent thermal resistance, R_j, for each thermally inhomogeneous layer is calculated using the following equation:

$$1/ R_j = f_a/ R_{aj} + f_b/ R_{bj} + \ldots + f_q/ R_{qj} \qquad [11]$$

Where:

$R_{aj}, R_{bj} \ldots \ldots R_{qj}$ are the thermal resistance of fractional areas $f_a, f_b \ldots f_q$ of layer j.

The lower limit of the thermal resistance is determined by using the following equation:

$$R''_T = R_{si} + R_1 + R_2 + \ldots + R_n + R_{se} \qquad [12]$$

(c) Estimation of Error

The maximum relative error in thermal transmittance or U-value, n, calculated as a percentage, is:

$$n = ((R'_T - R''_T)*100)/ (2 R_T) \qquad [13]$$

Using the aforementioned method, the design U-value of five different wall types were determined. Table 4 shows the thermal conductivity and thermal resistance of the various layers of the wall types and Table 5 show the calculated design U-values of the wall types. It is worth mentioning that the installer calculated U-value of the Concrete Block Masonry was 0.15 W/m^{2}K using their own methodology as opposed to our calculated value of 0.19 W/m^{2}K.

Table 4. Thermal conductivity/ resistance of different layers of the wall systems.

Layers	Thermal Conductivity (W/mK)	Thermal Resistance (m^{2}K/W)
Perforated board	0.13	
Oriented Strand Board (OSB)	9	
Plaster Board	0.21	
Hemp-lime	0.07	
PIR Insulation	0.02	
Wood Fibre Insulation 1	0.038	
Wood Fibre Insulation 2	0.041	
Mineral Wool Insulation	0.038	

Autoclaved Aerated Concrete (AAC) Block	0.16	
Concrete block dense	1.13	
Mortar (Outer)	0.94	
Mortar ((Inner)	0.88	
Timber Stud	0.12	
Internal surface resistance		0.13
External surface resistance		0.04
Cavity ventilated		0.13
Cavity slightly ventilated		0.18
Cavity unventilated		0.18

Table 5. Design U-value of the wall systems.

Wall System	Design U-Value (W/m^{2}K)
Concrete Block Masonry	0.19 (0.185)
Hempcell	0.15 (0.146)
PIR Wall	0.15 (0.150)
Wood Fibre Wall	0.15 (0.147)
Mineral Wool Wall	0.15 (0.145)

3.3.2. In situ Method

In this paper, only one method is considered for determining the in-situ U-value from heat flux and temperature difference. A detailed analysis of the effect of dynamic conditions on the U-value will be reported in a follow-up study. ISO 9869 [46] outlines the method for in-situ measurement of U-value of the building elements. U-value is obtained by dividing the mean density of heat flow rate by the mean internal and external temperature difference. The required data are acquired over a long period of time, i.e. more than 72 hours' data for a heavy weight structure and at least three nights' data for a lightweight structure. The U-value is determined from the following equation:

$$U = \frac{\sum_{j=1}^{n} q_j}{\sum_{j=1}^{n} (T_{ij} - T_{ej})} \qquad [14]$$

Where:

U is thermal transmittance (W/m^{2}K)

q is density of heat flow rate (W/m^2)

T_i is interior ambient temperature (°C)

Te is exterior ambient temperature (°C).

In this paper the term 'equivalent U-value' is used instead of 'U-value' in relation to the in situ measurements to account for the added effect of relative humidity, enthalpy flow and phase change on heat flux through the building envelope.

4. Result and discussion

4.1. Heat loss coefficients of the test buildings

The linear and multiple linear regression plots for Methods 1-5 are presented in Figs. 11-15. In Fig. 11, the daily energy use corrected for infiltration heat loss is plotted against the daily averaged temperature difference between the interior and exterior. The effect of solar heat gain and long wave radiation loss are not considered in the HLC calculation. The result of the Method 1 shows that the HLC of the Concrete Block Masonry is the highest and that of the mineral wool test building is the lowest. The HLC of the HempCell test building is second to the concrete block masonry. The large intercepts in the plots of, HempCell, PIR and Mineral Wool indicate the presence of other factors in addition to temperature difference influencing the heat input.
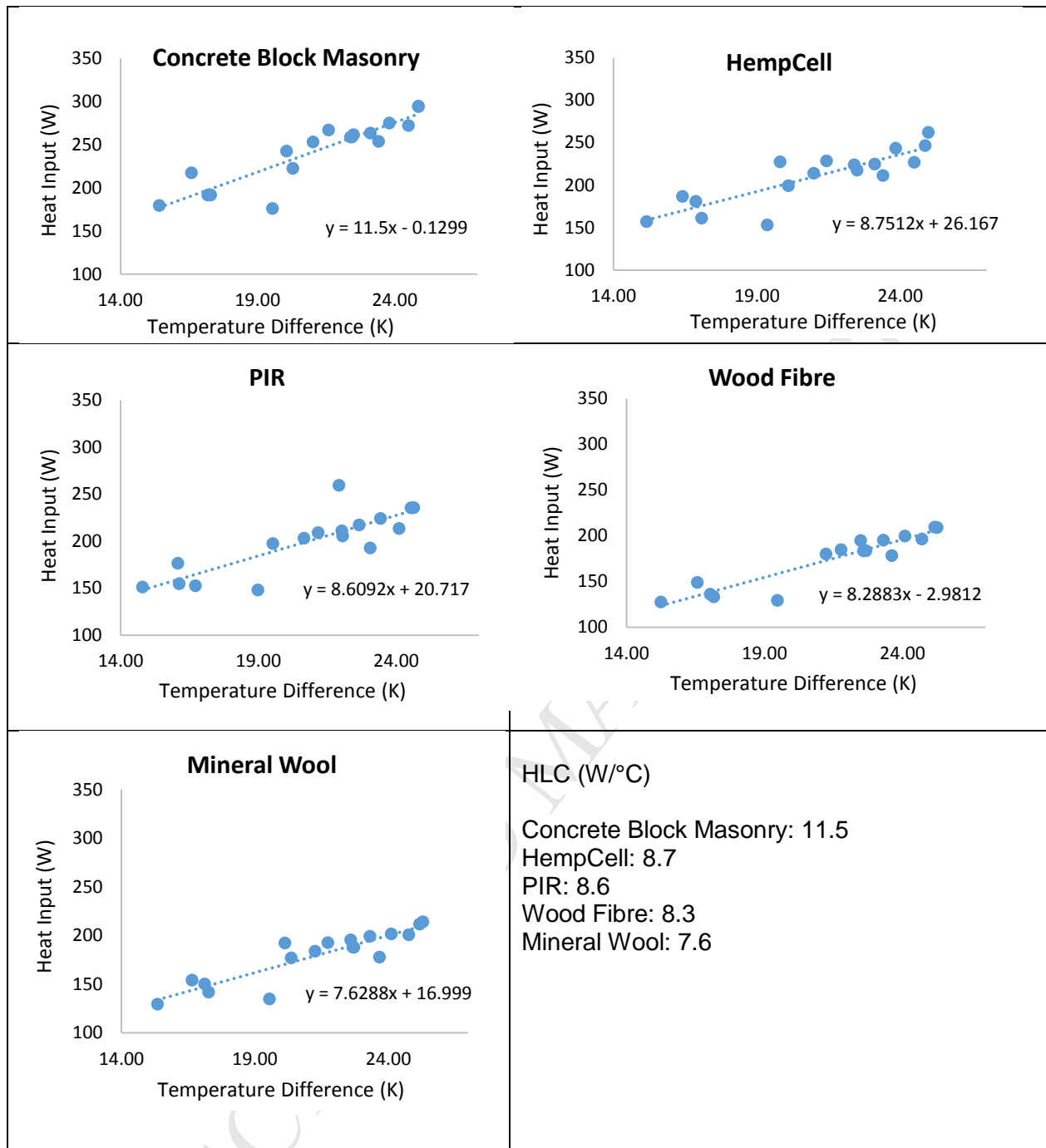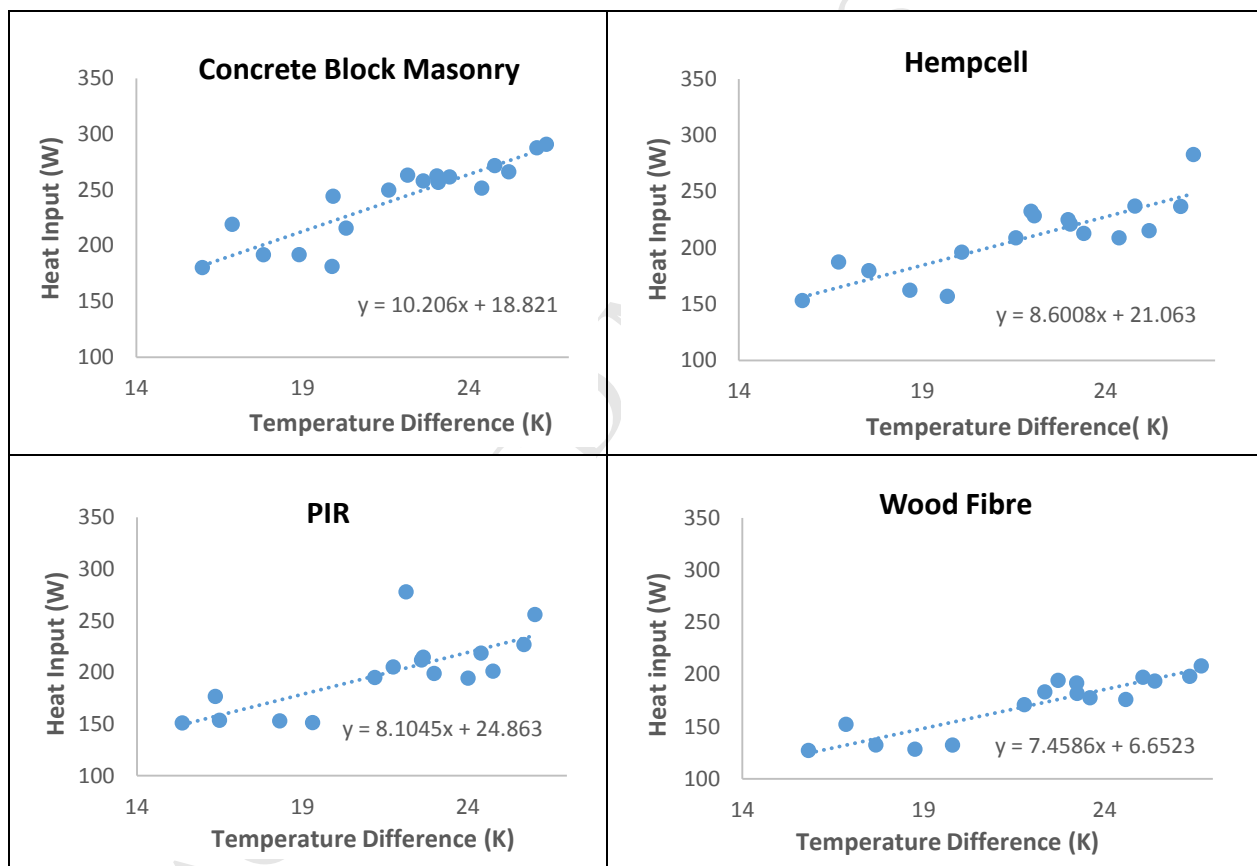
Fig. 11. Coheating regression plot using Method 1.

Fig.12 shows the coheating plots for Method 2. As discussed earlier, Method 2 employed only the night time data to minimise the effect of solar gain which also reduced the data point by 50%. For Concrete Block Masonry and Wood Fibre test buildings, noticeable decrease in HLC value of 12.7% and 10.7%, respectively, was observed. In Method 1 analysis, coheating plots of only these two buildings showed negative intercepts meaning that there was some possible heat gain from other

sources. In the method 2 plots, both intercepts became positive, although not as significant in case of Wood Fibre test building as in Concrete Block Masonry. It is plausible that there was stronger thermal storage effect in both panels due to the density and heat capacity of their core materials and therefore less heating energy was required in the night time while there was also heat loss by other means occurring at the same time in the Concrete Block Masonry. It should be further noted that the variation in number of data points between Method 1 and Method 2 may also have influenced the aforementioned variations in the HLC results.
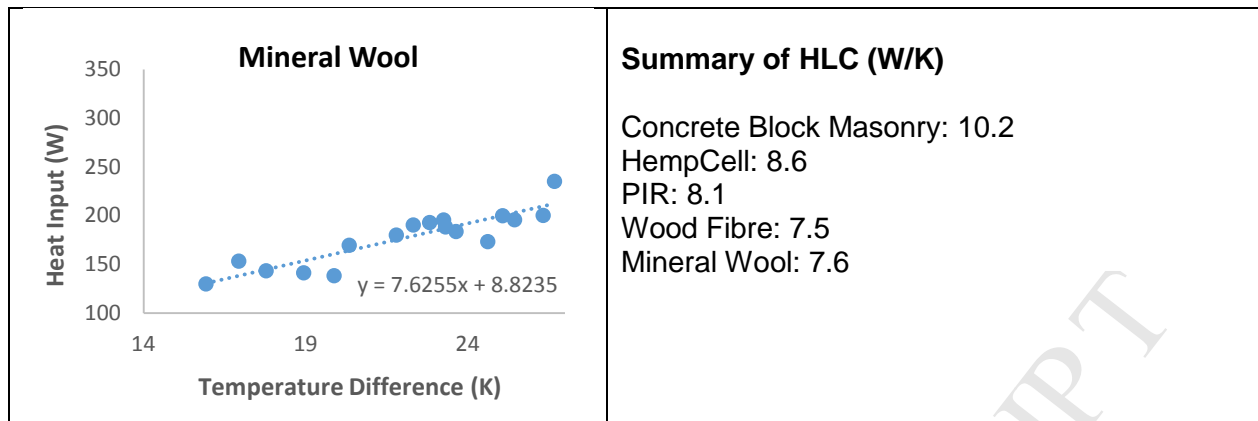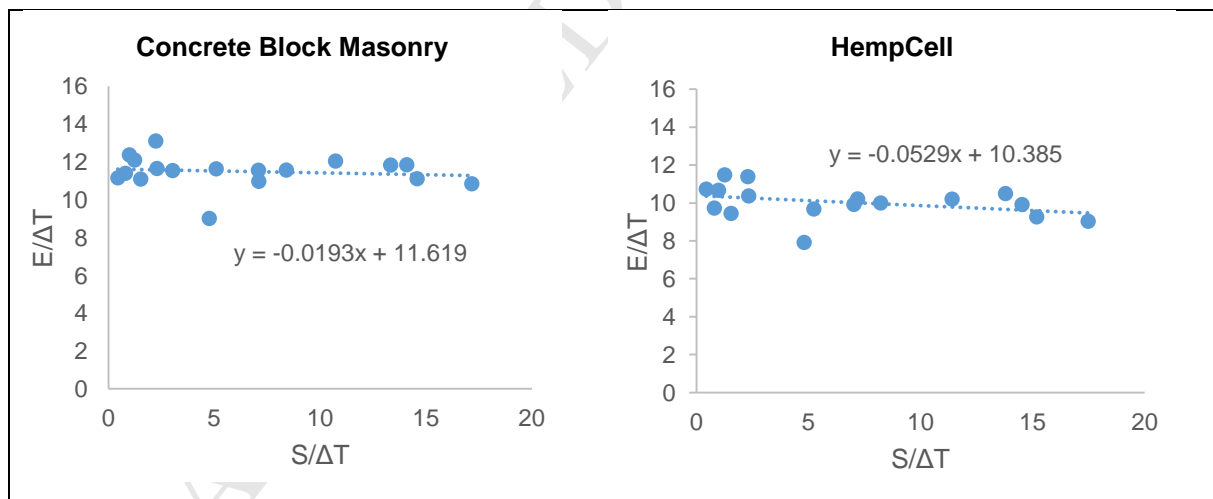
Fig. 12. Coheating regression plot using Method 2.

The outcomes obtained from applying Method 3 are shown in Fig.13. The constant term in the Siviour plots represents the HLC and the absolute value of the slope represents the effective solar aperture [40]. The effective solar aperture values can be used in Method 5 to determine the solar heat gains from the acquired data of solar irradiance [42]. The comparative trend of HLC values is similar to the previous findings: the HLC of the Concrete Block Masonry is the highest and that of the Wood Fibre is the lowest.
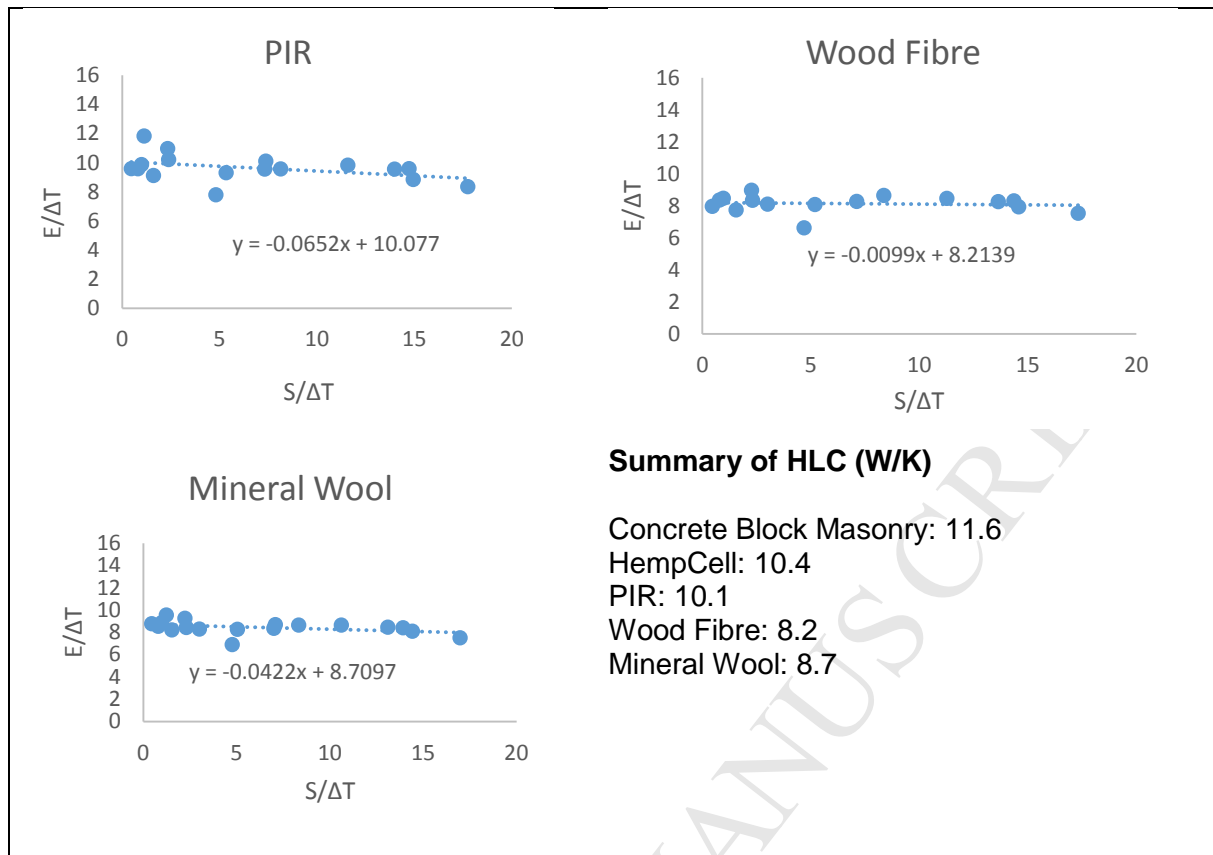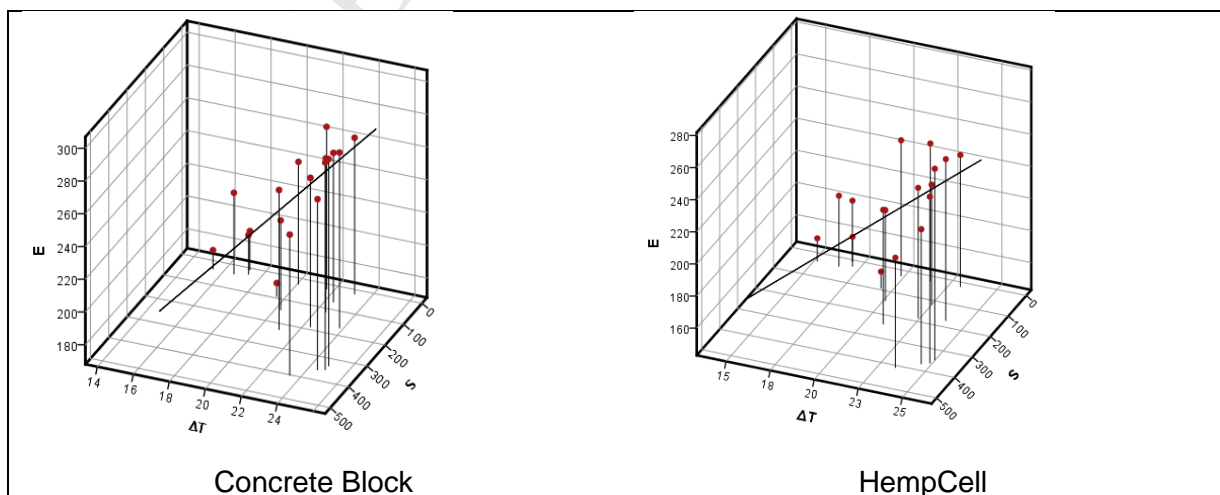
Fig. 13. Coheating regression plot using Method 3.

The results of the multiple linear regression, based on Method 4, where both solar irradiance and temperature difference were treated as independent variables and energy use as the dependent variable, are shown in Fig.14. The HLC values followed the same order as in the previous methods, with the highest HLC attributed to Concrete Block masonry and the lowest to the Wood Fibre.
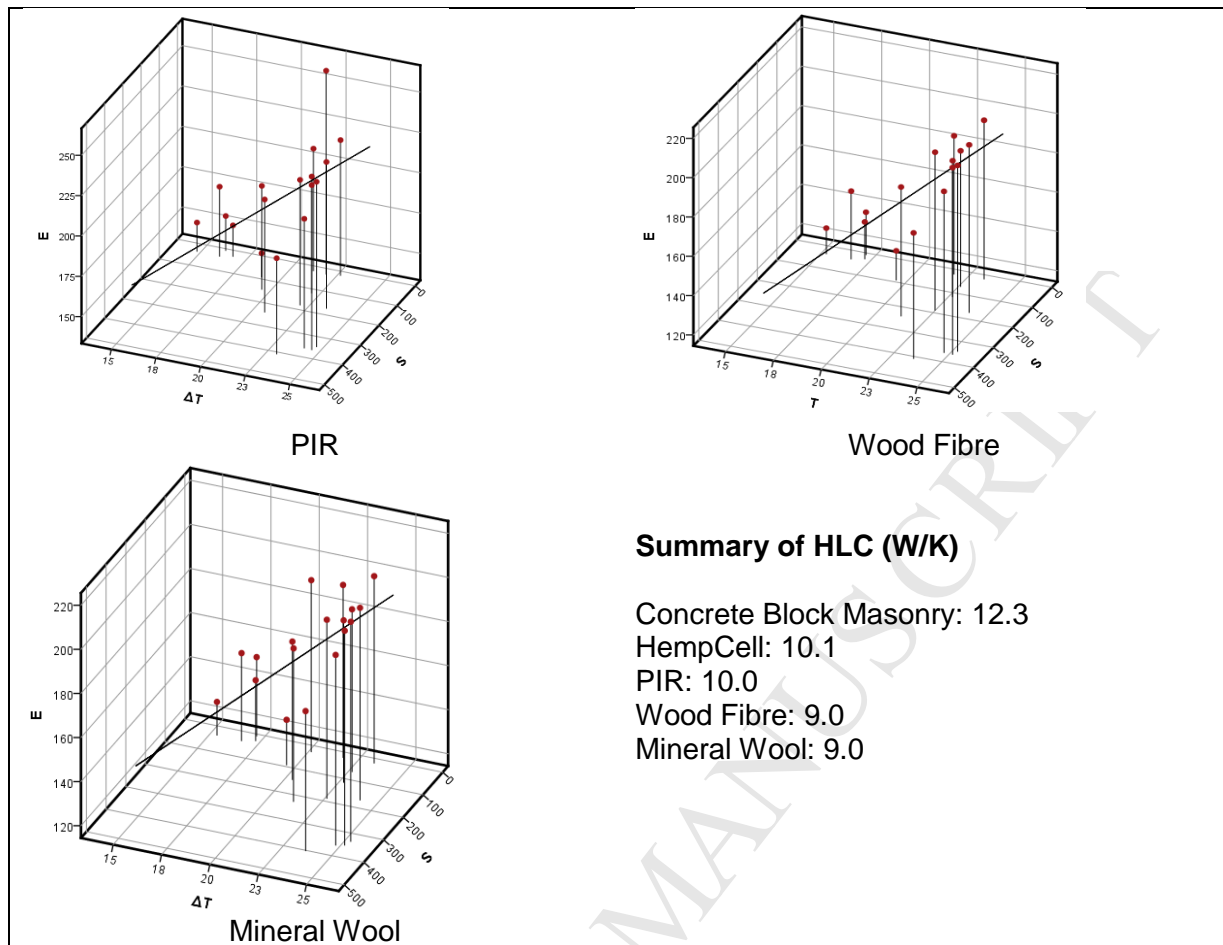
PIR

Wood Fibre

Summary of HLC (W/K)

Concrete Block Masonry: 12.3
HempCell: 10.1
PIR: 10.0
Wood Fibre: 9.0
Mineral Wool: 9.0

Mineral Wool

Fig. 14. Coheating regression plot using Method 4.

Fig. 15 shows the results based on Method 5, where the effect of solar gain was incorporated in the effective temperature difference and the effect of thermal mass was addressed by taking the temperature difference as an average of the present and previous time step. For the purpose of this method, averaged hourly data were analysed to determine the HLC values. Having deducted the infiltration heat loss from the total energy use and incorporated the effect of solar radiation, long wave radiation and thermal mass in terms of the effective temperature difference, it was assumed that the regression line could be forced through the origin of the axis. Thus, the infiltration corrected energy loss could be attributed to the solar corrected temperature difference.
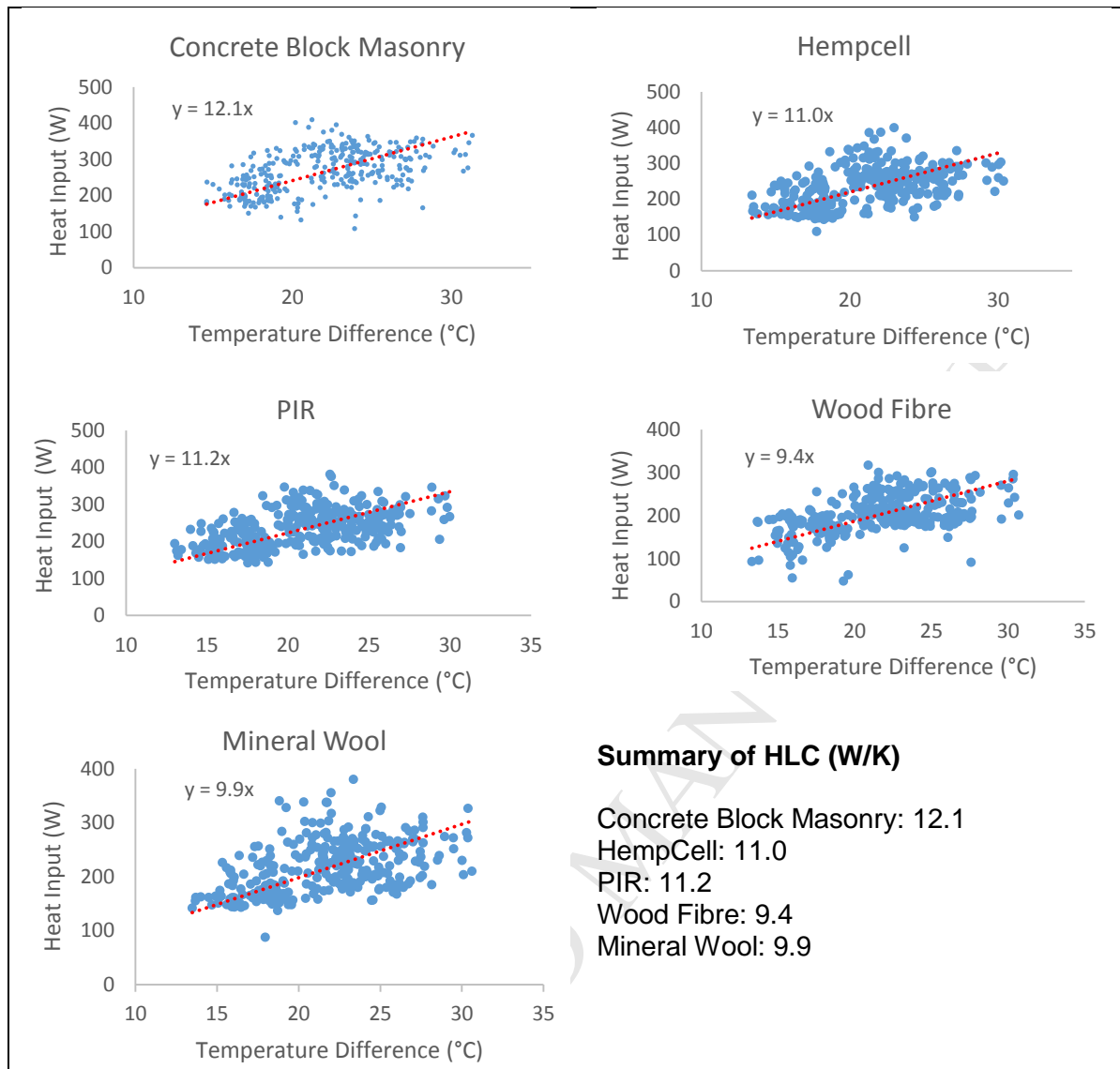
Fig. 15. Coheating regression plot using Method 5.

HLC values derived by all five methods and by the simplified heat loss calculation are presented in Fig.16. The average values based on the five methods are presented in Fig.17. The HLC values obtained by using Method 5 are lower than the corresponding simplified calculated values by 0%- 41.6%. A difference of 10% between the calculated and experimentally determined values of HLC has been reported previously as typical [47]. Except for the Concrete Block Masonry, all other HLC values, therefore, are in good agreement with the calculated values. Although Method 5 provides more agreeable result to the calculated HLC values than the other methods, this is very time consuming to determine the $\Delta T_{a.Effective}$. In general,

Method 3 and Method 4 are more preferred as they are easy to calculate and provides reliable result in most of the cases [40, 42, 43].

It is worth noting, with regards to comparing HLC values derived from different methods, that the number of data points are note same across the methods. For example, the number of night time data point for Method 2 is 50% of that of the day-night data points for Method 1. Furthermore, Method 5 utilised averaged hourly data instead of averaged daily data, thus using significantly more data points than the other methods. The variations of the data resolution between different methods may have contributed to the difference in the HLC results between the methods.
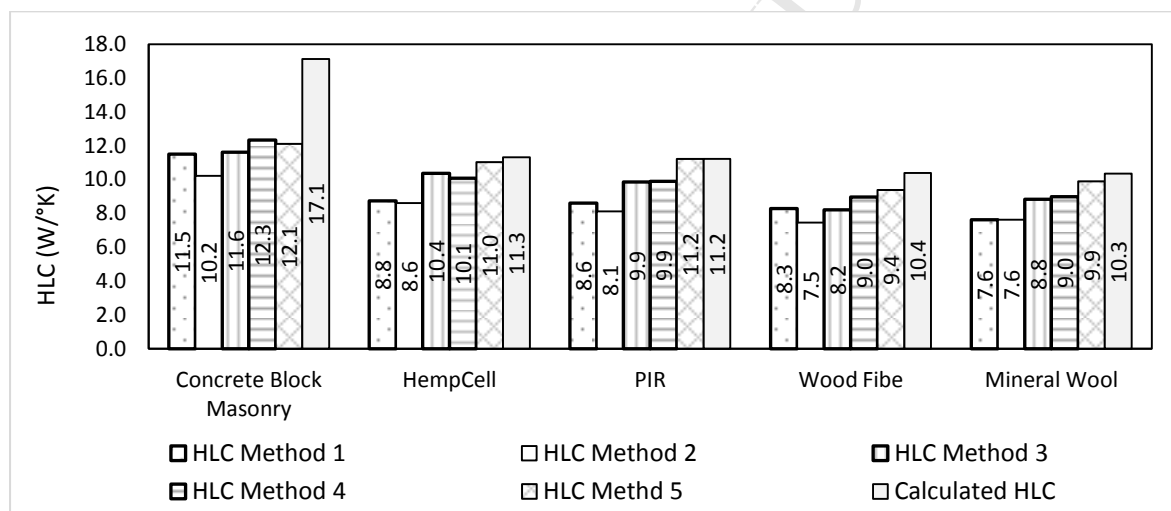

Fig. 16. The experimental and calculated HLC values.

The average value of HLC, as shown in Fig.17, may only be meaningful in terms of comparing the performance of different test buildings. The average HLC values of the Concrete Block, HempCell, PIR and Mineral Wool are 36.5%, 15.4%, 12.7%, and 1.6% higher than that of Wood Fibre, respectively.
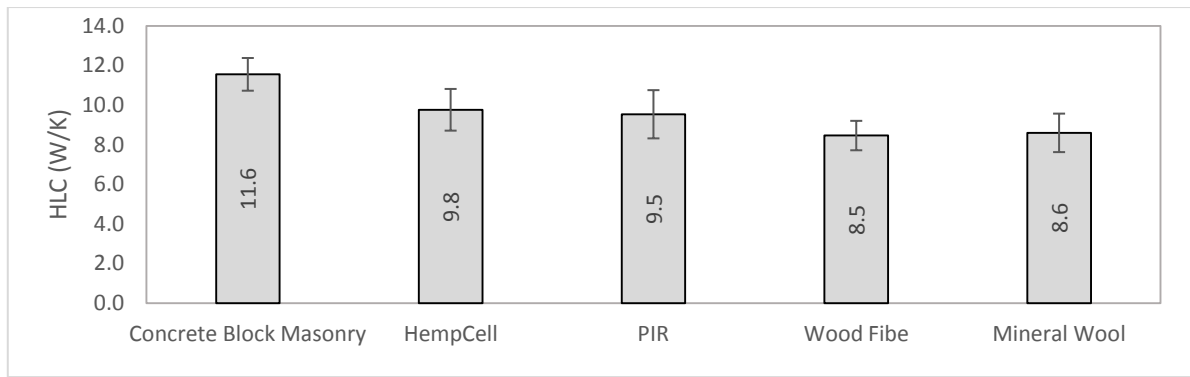
Fig. 17. The Average HLC values of the test buildings.

4.2. Equivalent U-values of the test buildings

The result of the equivalent U-value, based on day–night and night time data, along with the design U-value, HLC values for Method 5 and the calculated HLC values are shown in Fig. 18. During the U-value measurements, the minimum ambient temperature difference between the interior and exterior of the test buildings was 15 K, the average temperature difference during the whole day-night period was 21 K and during the night time was 21.8 K. The data were acquired for 18 days. Thus both temperature difference and monitoring period were favourable for reliable data acquisition as far as determining in situ U-value is concerned [33, 46]. The U-values of HempCell, PIR, Mineral Wool and Wood Fibre are marginally lower than their design U-values. While determining in situ U-value of timber frame walls incorporating bio-based and mineral insulations, similar observations that in situ U-value could be slightly lower or equal to that of manufacturer's declared value were also made in a number of in situ studies [20, 45, 48]. However, the U-value of concrete Block Masonry is 32.8% higher than their design U-values. In two separate studies, Building Research Establishment (BRE) reported 29-34% [49] and 104% [50] higher U-value than the calculated U-value of insulated and partially insulated masonry cavity walls, respectively. The reasons for higher U-value of Concrete Block

Wall may be attributed to its absorbed moisture content during the construction phase, thermal bridge through the mortar joints and possible convection current in the cavity wall. It can be further observed that the order of the HLC values, both for Method 5 and calculated one, follows that of the equivalent U-values.
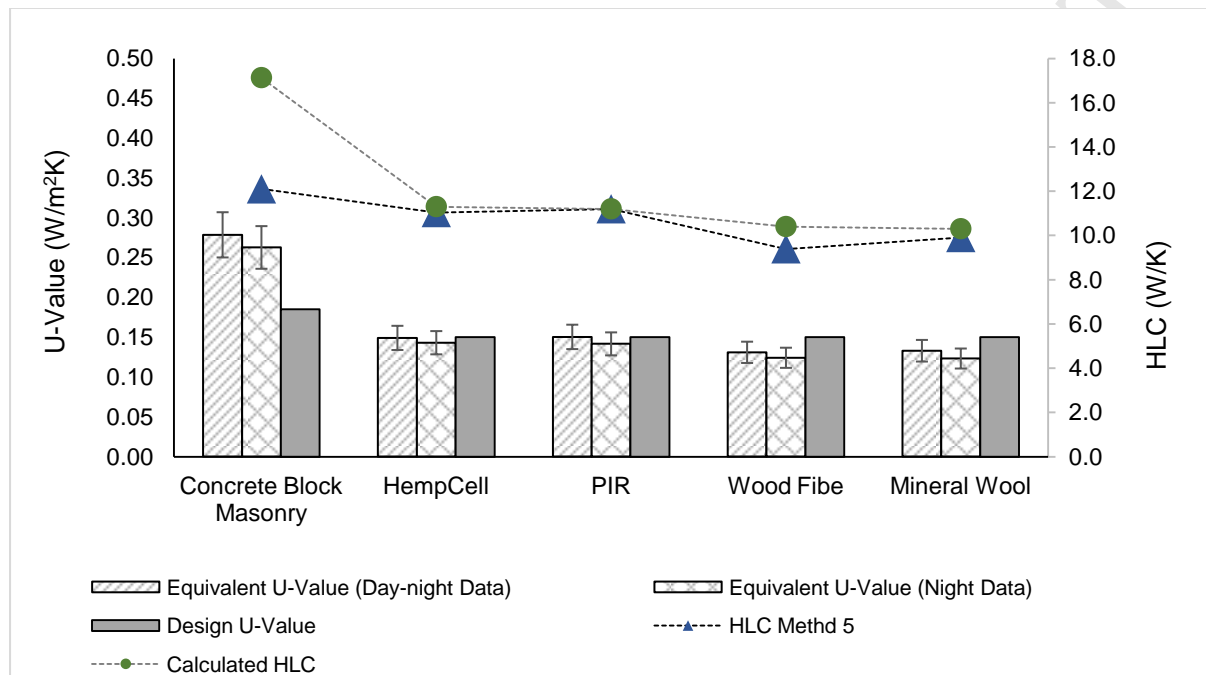

Fig. 18. The in situ U-values, design U-values of the wall systems and calculated HLC and HLC by method 5.

5. Conclusion

Comparative coheating tests have been carried out in five test buildings: one with a masonry wall system constructed of Concrete Blocks and four with timber-frame wall panels insulated with Hemp-lime composite, PIR, Wood Fibre and Mineral Wool, respectively. Five different analysis methods were applied to the coheating data to determine their HLCs. While variability was observed between the outcome of the methods in terms of the HLC values, the hierarchy of the values among the test buildings was consistent, with Concrete Block exhibiting the highest and Wood Fibre exhibiting the lowest HLC value. Except for Concrete Block Masonry, good agreement was found between the HLC values determined by applying Method 5,

where the analysis incorporated both the effects of solar radiation and thermal mass, and the corresponding calculated values. In terms of the in situ U-value determined by the average method, Concrete Block wall exhibited 32.8% higher U-value than its design value while the other wall systems showed marginally lower U-values than their corresponding design values. The reasons for higher U-value of Concrete Block Wall may be attributed to its absorbed liquid water content during the construction phase, thermal bridge through the mortar joints and possible convection current in the cavity wall. The fact that the equivalent U-value of the HempCell system remained lower than its design U-value demonstrates that the pre-dried and prefabricated Hempcell panel can thermally perform to its optimal level from the very beginning of its installation as opposed to a hemp-lime wall cast onsite that takes more than 6 months to perform optimally.

Acknowledgements

References

[1] I.E. Agency, Energy Efficiency Market Report 2015: Market Trends and Medium-Term Prospects, 2015.
[2] Directive 2010/31/EU of the European Parliament and of the Council of 19 May 2010 on the energy performance of buildings, Official Journal of the European Union L 153(13) (2010) 13–35.
[3] Directive 2012/27/EU of the European Parliament and of the Council of 25 October 2012 on energy efficiency, amending Directives 2009/125/EC and 2010/30/EU and repealing

Directives 2004/8/EC and 2006/32/EC Text with EEA relevance, Official Journal of the European Union L 315(1) (2012) 1-56.

[4] G. HM, Approved Document L1A: Conservation of Fuel and Power in New Dwellings. The Building Regulations 2010., in: H. Government (Ed.) NBS, London, 2013.

[5] A. Stafford, D. Johnston, D. Miles-Shenton, D. Farmer, M. Brooke-Peat, C. Gorse, Adding value and meaning to coheating tests, Structural Survey 32(4) (2014) 331-342.

[6] R. Galvin, Making the 'rebound effect' more useful for performance evaluation of thermal retrofits of existing homes: Defining the 'energy savings deficit' and the 'energy performance gap', Energy and Buildings 69 (2014) 515-524.

[7] O. Guerra-Santin, C. Tweed, H. Jenkins, S. Jiang, Monitoring the performance of low energy dwellings: Two UK case studies, Energy and Buildings 64 (2013) 32-40.

[8] D. Cal`ı, T. Osterhage, R. Streblow, D. Muller, Energy performance gap in refurbished German dwellings: lesson learned from a field test, Energy and Buildings (2016).

[9] P. deWilde, The gap between predicted and measured energy performance of buildings: A framework for investigation, Automation in Construction 41 (2014) 40-49.

[10] A.C. Menezes, A. Cripps, D. Bouchlaghem, R. Buswell, Predicted vs. actual energy performance of non-domestic buildings: Using post-occupancy evaluation data to reduce the performance gap, Applied Energy 97 (2012) 355-364.

[11] H. Hens, Energy efficient retrofit of an end of the row house: Confronting predictions with long-term measurements, Energy and Buildings 42(10) (2010) 1939-1947.

[12] H. Erhorn, Bedarf – Verbrauch: Ein Reizthema ohne Ende oder die Chance fürsachliche Energieberatung?

[13] C.A. Gorse, D. Glew, D. Miles-Shenton, D. Farmer, M. Fletcher, BUILDING PERFORMANCE: FABRIC, IMPACT AND IMPLICATIONS, Sustainable Building 2013 Hong Kong Regional Conference:

Urban Density & Sustainability, Hong Kong, 2013.

[14] K.B. Janda, Buildings don't use energy: people do, Architectural science review 54(1) (2011) 15-22.

[15] O. Guerra Santin, Behavioural Patterns and User Profiles related to energy consumption for heating, Energy and Buildings 43(10) (2011) 2662-2672.

[16] Z.M. Gill, M.J. Tierney, I.M. Pegg, N. Allan, Low-energy dwellings: the contribution of behaviours to actual performance, Building Research & Information 38(5) (2010) 491-508.

[17] P. Chastas, T. Theodosiou, D. Bikas, Embodied energy in residential buildings-towards the nearly zero energy building: A literature review, Building and Environment (2016).

[18] F. Myersa, R. Fullera, R.H. Crawfordb, The potential to reduce the embodied energy in construction through the use of renewable materials, ASA012: Building on knowledge, theory and practicd: Proceedingsof the 46th Annual Conference of the Architectural Science Association, Goldcost, Qld., 2012, pp. 1-8.

[19] A. Cripps, Crops in construction handbook, CIRIA, London, 2004.

[20] E. Latif, M.A. Ciupala, S. Tucker, D.C. Wijeyesekera, D.J. Newport, Hygrothermal performance of wood-hemp insulation in timber frame wall panels with and without a vapour barrier, Building and Environment 92 (2015) 122-134.

[21] E. Latif, M. Lawrence, A. Shea, P. Walker, Moisture buffer potential of experimental wall assemblies incorporating formulated hemp-lime, Building and Environment 93 (2015) 199-209.

[22] E. Latif, S. Tucker, M.A. Ciupala, D.C. Wijeyesekera, D.J. Newport, M. Pruteanu, Quasi steady state and dynamic hygrothermal performance of fibrous Hemp and Stone Wool insulations: Two innovative laboratory based investigations, Building and Environment 95 (2016) 391-404.

[23] A. Takano, S.K. Pal, M. Kuittinen, K. Alanne, M. Hughes, S. Winter, The effect of material selection on life cycle energy balance: A case study on a hypothetical building model in Finland, Building and Environment 89 (2015) 192-202.

[24] L. Zampori, G. Dotelli, V. Vernelli, Life Cycle Assessment of Hemp Cultivation and Use of Hemp-Based

Thermal Insulator Materials in Buildings, Environmental Science and Technology 47 (2013) 7413–7420.

[25] P. Daly, P. Ronchetti, T. Woolley, Hemp Lime Bio-composite as a Building Material Irish Construction, Environmental Protection Agency, Ireland, 2012.

[26] A. Sutton, D. Black, P. Walker, Hemp lime: An introduction to low impact building materials, in: B.R. Establishment (Ed.) IHS BRE Press, Garston, Watford, 2011.

[27] J. Zach, A. Korjenicb, V. Petranek, J. Hroudova, T. Bednar, Performance evaluation and research of alternative thermal insulations based on

sheep wool, Energy and Buildings 49 (2012) 246-253.

[28] U.o. Bath, HEMPSEC: pre-fabricated, pre-dried panelised system of hemp-lime construction. <www.hempsec.eu>, (accessed 10.07.2015.2015).

[29] BOPAS, Hempcell System. <http://www.bopas.org/technologies/view/48/Hempcell%20System>, 2016).

[30] E. Latif, S. Tucker, M.A. Ciupala, D.C. Wiyjeyesekera, D. Newport, Hygric Properties of Five Hemp Bio-Insulations with Differing Compositions, Construction and Building Materials 66(C) (2014) 702-711.

[31] D. Johnston, D. Miles-Shenton, D. Farmer, M. Brooke-Peat, Post-construction thermal testing: some recent measurements, Proceedings of the Institution of Civil Engineers-Engineering Sustainability, Thomas Telford Ltd, 2015, pp. 131-139.

[32] J. Wingfield, D. Johnston, D. Miles-Shenton, M. Bell, Whole House Heat Loss Test Method (Coheating), Leeds Metropolitan University, 2010.

[33] G. Desogus, S. Mura, R. Ricciu, Comparing different approaches to in situ measurement of building components thermal resistance, Energy and Buildings 43(10) (2011) 2613-2620.

[34] L. Evangelisti, C. Guattari, P. Gori, R. Vollaro, In Situ Thermal Transmittance Measurements for Investigating Differences between Wall Models and Actual Building Performance, Sustainability 7(8) (2015) 10388-10398.

[35] U.o. Bath, The HIVE. <http://www.bath.ac.uk/research/centres/brp/hive/>, 2014).

[36] B.S. Institute, BS EN ISO 6946. Building components and building elements. Thermal resistance and thermal transmittance. Calculation method, 2007.

[37] Farnell, Betatherm data sheet. <http://www.farnell.com/datasheets/69441.pdf>, 2016 (accessed 01.09.16.2016).

[38] Farnell, HIH-4000 series: Humidity sensors. <http://www.farnell.com/datasheets/1685535.pdf>, 2016 (accessed 01.01.16.2016).

[39] Hukseflux, HFP01 Heat flux plate. <http://www.hukseflux.com/product/hfp01?referrer=/product_group/heat-flux-sen>, 2016 (accessed 10.09.16.2016).

[40] G. Bauwens, S. Roels, Co-heating test: A state-of-the-art, Energy and Buildings 82 (2014) 163-172.

[41] Minneapolis Blower Door™ Operation Manual for Model 3 and Model 4 Systems, The Energy Conservatory, 2012.

[42] D. Butler, A. Dengel, Review of co-heating test methodologies, Milton Keynes, 2013.

[43] R. Everett, A. Horton, J. Doggart, Linford Low Energy Houses, Energy Research Group, Open University., UK, 1985.

[44] W. Feist, Passive House Planning Package Passive House Institute, Germany, 2015.

[45] E. Latif, M.A. Ciupala, D.C. Wijeyesekerac, The comparative in situ hygrothermal performance of Hemp and Stone Wool insulations in vapour open timber frame wall panels, Construction and Building Materials 73 (2014) 205-213.

[46] ISO 9869. Thermal insulation-Building elements -In-situ measurement of thermal resistance and thermal transmittance, International Organization for Standardization, Switzerland, 1994.

[47] D.K. Alexander, H.G. Jenkins, The Validity and Reliability of Co-heating Tests Made on Highly Insulated Dwellings, Energy Procedia 78 (2015) 1732-1737.

[48] A. Nicolajsen, Thermal transmittance of a cellulose loose-fill insulation material, Building and Environment 40 (2005) pp. 907-914.

[49] J. Hulme, S. Doran In-situ measurements of wall U-values in English housing, 2014.

[50] S. Doran, DETR Framework Project Report: Field investigations of the thermal performance of construction elements as built, 2000.

- Test buildings of different wall systems are compared by coheating tests.
- Five methods applied to analyse the coheating data.
- Masonry wall exhibited the highest deviation from the design U-value
- Except for masonry, heat loss coefficients, U-values of the systems are similar.
- Heat loss coefficient values can differ based on the methods applied.